PHYSICAL REVIEW B VOLUME 19, NUMBER 4 15 FEBRUARY 1979

Linearized augmented plane-wave method for the electronic band structure of thin films

H. Krakauer and M. Posternak
Department of Physics and Astronomy, Northwestern University, Evanston, Illinois 60201

A. J. Freeman
Department of Physics, and Astronomy, Northwestern University, Evanston, Illinois 60201
and Argonne National Laboratory, Argonne, Illinois 60439
(Received 31 July 1978)

We present a new method for treating the electronic structure of thin films which is based on a generalization of the bulk linearized augmented-plane-wave (LAPW) method. This method avoids using the slab-superlattice geometry and combines the advantages of energy-independent muffin-tin Hamiltonian methods [fast root evaluation and rapid convergence for d-band metals as well as for nearly-free-electron (NFE) crystals] with the simple matrix element determination of the original augmented plane-wave (APW) method. As in the bulk LAPW method, the asymptote problem of the APW method is avoided, and the basis functions are everywhere continuous and differentiable. In addition, the film LAPW method retains such desirable features of the APW method as the ability to treat general potentials with no shape approximations, the ease with which relativistic effects can be included, and the fact that the basis size does not increase substantially for heavier elements. As a first application and test of the method, non-self-consistent calculations are performed in the local-density approximation for exchange and correlation and with the one-electron potential constructed from a superposition of atomic charge densities. A semirelativistic formulation is employed in which the Dirac equation is solved in the limit of zero spin-orbit coupling inside the muffin-tin spheres. Results are reported for up to five atomic layer thin films (slabs) of the transition metals Fe, Co, Ni, and Cu and a nine-layer film of the NFE metal Al. The results are in generally good agreement with other theoretical calculations. Some trends in the transition-metal band structures are discussed. A surface-state surface-resonance band for Al(001) is found to completely account for and clarify behavior observed in very recent photoemission measurements.

I. INTRODUCTION

Studies of surface electronic phenomena have made rapid advances in recent years mostly because of (i) the development of novel powerful experimental methods and theoretical computational schemes, and (ii) the strong interaction which has developed between them. On the experimental side, the development of high-vacuum techniques for the preparation of stable and well-controlled surfaces together with high-resolution spectroscopic and other methods[1-4] for studying surface phenomena have provided (in many cases) a wealth of reproducible experimental data for a variety of materials, notably, the important free-electron metals, semiconductors and transition metals. On the theoretical side, a variety of powerful and successful energy-band methods for treating bulk structures have been adapted for the study of the electronic structure of surfaces.[5-20]

Regardless of the geometrical model used to represent the surface (thin-film or slab geometry, slab-superlattice geometry or the semi-infinite crystal), the many different theoretical approaches have one feature in common: they all face the necessity of treating large unit cells containing many inequivalent atoms. For such calculations, reciprocal lattice or plane-wave (PW) based methods enjoy an important advantage, namely, simple matrix element determination and corresponding ease of programming. Of the PW methods, only pseudopotential[6,7,14] or supplemented-orthogonalized plane wave (OPW)-type[8,15] calculations have been performed to date. For treating d-band systems, these methods[8,14,15] have primarily relied on a slab-superlattice geometry[21] in which the slab is periodically repeated and separated from adjacent slabs by several layer spacings of vacuum. In this manner periodicity is artificially retained normal to the slab, thus permitting the use of standard bulk electronic methods. Aside from the usual difficulties associated with pseudopotential methods, there are two disadvantages in this approach. Because of the large size of the perpendicular lattice parameter (the sum of the slab thickness plus the thickness of the vacuum region), convergence of the basis in reciprocal lattice space can be made significantly worse if many vacuum layers are required to prevent the slabs from interacting with each other. In addition, the PW-type basis is required to yield the correct behavior of the wave function inside the slab as well as to

correctly represent the decay into vacuum.

In this paper we present[22] a new method for treating thin films which avoids the above-mentioned difficulties, is very accurate, and suffers little, if any, loss in computational speed compared to pseudopotential methods. This method is based on a generalization of the bulk linearized augmented plane-wave (LAPW)[23,24] method and combines the advantages of energy-independent muffin-tin (MT) Hamiltonian methods[12,16,23] [fast root evaluation and rapid convergence for d-band metals as well as for nearly-free-electron (NFE) crystals] with the simple matrix-element determination of the original APW[25] method. The full one-electron potential is used and is constructed using the local-density approximation[26] for exchange and correlation. The main advantages of the LAPW method over the APW method are: (i) The secular determinant is linear in energy, which permits the simultaneous determination of both eigenvalues and eigenvectors by standard matrix diagonalization with very little loss of accuracy. (ii) Singularities in the matrix elements are eliminated, i.e., the asymptote problem of the APW method is avoided. (iii) The basis functions are everywhere continuous and differentiable. In addition, the LAPW method retains such desirable features of the APW method as the ability to treat general potentials with no shape approximations, the ease with which relativistic effects can be included, and the fact that the basis size does not increase substantially for heavier elements.

The characteristic feature of the bulk (L)APW method is that a PW basis function in the interstitial region (where variations in the potential are relatively smooth) is augmented inside the MT spheres by functions constructed from the exact solutions in these spheres (where variations in the potential are large). By an extension of this idea to the film geometry and using the film-muffin-tin (FMT)[10,11,16] potential, a suitably defined PW basis function in the interstitial region of the slab is additionally augmented in the vacuum region by functions constructed from the exact solutions of Schrödinger's equation (SE) there. In the film-LAPW formalism, the two vacuum regions (above and below the film) are treated in a manner which is completely analogous to the MT spheres. There is no problem in optimizing the thickness of the vacuum region; to obtain the solutions of SE in this region we essentially integrate SE inward from $\pm\infty$. We want to emphasize that the FMT potential is used only for the purpose of constructing the film-LAPW basis functions. Once defined, however, this basis can be used to treat general potentials with no shape approximations.

The formalism for the film-LAPW method is presented in Sec. II and in the Appendix. Some results using this method are presented in Sec. III. As a first application, and test of the method, calculations for Fe, Co, Ni, Cu, and Al were performed, these being representative of d-band and NFE-like metals.[22] A semirelativistic formulation[27] is used in which Dirac's equation is solved in the limit of zero spin-orbit coupling inside the MT spheres. Results for one-, three-, and five-layer Cu (001) films are found to be in good agreement with other theoretical calculations for thin films and for bulk. Effects due to the neglect of self-consistency are discussed, and it is found that, as in bulk calculations, adjusting the value of the exchange-correlation parameter can lead to results (for the band eigenvalues) which are close to those obtained self-consistently. Some trends in the transition-metal band structures are discussed.

Although the aluminum calculation was originally performed primarily to test the method and to demonstrate the wide range of the applicability, we subsequently found[28] that we could completely account for and clarify behavior observed in a very recent photoemission measurement[29] of an occupied surface state (SS) *and* surface resonance on clean Al (001). Essential aspects of these measurements, which could not be understood by comparing with previously calculated band structures,[30,31] are reproduced and accounted for by results obtained for a nine-layer Al film. In particular, we find a SS-surface resonance "band" which agrees very well with the measured dispersion relation.

II. FORMALISM

The LAPW basis functions are obtained from solutions of the FMT potential. It must be emphasized, however, that this potential is used only for the purpose of constructing the basis functions; once defined, these basis functions can be used to treat general potentials with no shape approximations. The FMT potential is schematically depicted in Fig. 1. While we restrict ourselves to films with z-reflection symmetry, this is not a requirement of the method. Since the film is periodic in the x-y plane and nonperiodic normal to the film (the z-direction), a unit cell can be defined extending to $\pm\infty$ in the z-direction, as indicated by the dashed lines in Fig. 1. Inside the muffin-tin spheres (region I) the potential is spherically symmetric; in the interstitial region (region II) the potential is constant. Finally, in the exterior or vacuum region (region III is defined by planar boundaries at $\pm\frac{1}{2}D$) the potential is dependent only on z.

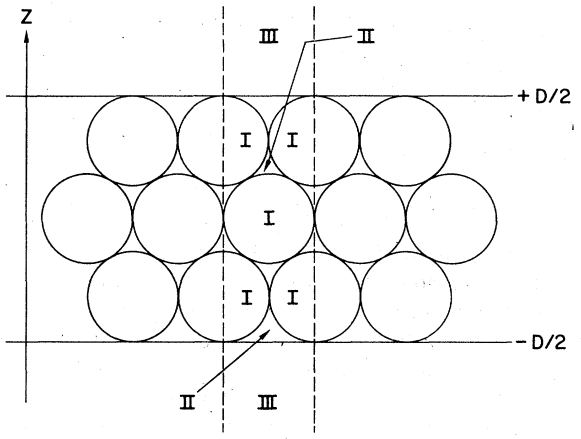

FIG. 1. Schematic representation of the film-muffin-tin (FMT) potential for a three-layer film. The unit cell, indicated by dashed lines, extends to $z = \pm\infty$. There are two boundary planes at $z = \pm\frac{1}{2}D$.

A. LAPQ-basis functions

In analogy with the bulk (L)APW method, a plane-wave-like basis function in the interstitial region is augmented by functions constructed from exact solutions in the MT regions (I) and the exterior regions (III) of Fig. 1. These functions must be matched onto the plane-wave-like basis function (and its derivative) at the MT sphere surfaces and at the boundary planes at $z = \frac{1}{2}D$. The resulting basis functions are then everywhere continuous and differentiable.

1. Interstitial region

In the interstitial region the basis function is defined as a product of a two-dimensional plane-wave and a one-dimensional symmetrized plane wave:

$$\varphi_{m,n}(\vec{k},\vec{r}) = (2/\Omega)^{1/2}\exp[i(\vec{k}+\vec{g}_m)\cdot\vec{r}]\,x\begin{cases}\cos(k_n z); (+)\\ \sin(k_n z); (-)\end{cases}. \tag{1}$$

Here (+) and (−) denote states which are, respectively, symmetric and antisymmetric with respect to z reflection; $\vec{k}$ is a two-dimensional crystal momentum vector, $\vec{g}_m$ is a two-dimensional reciprocal lattice vector, Ω equals the volume of the unit cell between $z = \pm\frac{1}{2}D$, and k_n is defined in terms of the distance D between the boundary planes:

$$k_n \equiv \begin{cases} n2\pi/D; & (+)\\ (n+\frac{1}{2})2\pi/D; & (-)\end{cases} \qquad n = 0,1,2,3,\ldots. \tag{2}$$

For the antisymmetric case, k_n is defined as shown in order to avoid having a node at the boundary plane.

There is a fair degree of freedom in the definition of k_n, since we require the plane-wave form of the basis function only for $|z| \leq \frac{1}{2}D$. Thus k_n could have been defined in terms of some other length $D' > D$. This in turn permits a redefinition of $k_n^{(-)}$, e.g., $k_n^{(-)} = n2\pi/D'$, since a node no longer automatically occurs at $z = \pm\frac{1}{2}D$ in this case. Other variations are possible. For example, in an independently developed version of a similar film LAPW formalism, Jepsen *et al.*[24] have defined $k_n^{(+)} = (n+\frac{1}{2})2\pi/D'$ and $k_n^{(-)} = n2\pi/D'(D' > D)$, thus forcing a node at $z = \pm\frac{1}{2}D'$ for both (+) and (−) states. This choice has the feature that there is no constant plane-wave in the basis set (in contrast to the situation in bulk). For the first test of our method, we have adopted the definition given by Eq. (2), since it slightly simplifies the matrix-element determination. On the other hand, this choice forces the first derivative, $\partial/\partial z$, to be zero at $z = \pm\frac{1}{2}D$. In future (particularly self-consistent) calculations we will test the effect of choosing $D' > D$.

2. Muffin-tin spheres

Inside the αth MT sphere in the unit cell, the basis function is expanded in spherical harmonics times a radial function and its energy derivative:

$$\varphi_{m,n}(\vec{k},\vec{r}) = \sum_L [A_{L,\alpha}(\vec{k})u_{l,\alpha}(E_l,r) + B_{L,\alpha}(\vec{k})\dot{u}_{l,\alpha}(E_l,r)]\times Y_L(\vec{r})\begin{cases} i^l & (+)\\ i^{l-1} & (-)\end{cases}, \tag{3}$$

where $\dot{u}(E_l) \equiv [\partial u/\partial E]_{E_l}$, $L \equiv \{l,m\}$, and E_l are constant energy parameters. The significance of using the energy derivative function is that to a good approximation the function $u_l(E)$ is linear over an energy range centered on E_l: $u_l(E) = u_l(E_l) + (E-E_l)\dot{u}_l(E_l)$.[23] The radial function u_l is obtained by solving the Dirac equation in the limit of zero spin-orbit coupling. We use a formulation developed by Koelling and Harmon[27] for solving the Dirac equation, which drops the spin-orbit interaction but allows all other relativistic kinematic

effects (mass velocity, Darwin and higher-order terms) to be included. The A_L and B_L coefficients are determined by matching onto Eq. (1) so that the basis function and its derivative are continuous across the MT-sphere boundary (cf. Appendix). Essentially because two radial functions are used, the LAPW method avoids the asymptote problem encountered in the conventional APW method. The constant energy parameters E_l are generally set equal to a value in the center of the energy range for the bands of that l character. The resulting band eigenvalues are very insensitive (typically over a range of about 1 Ry) to the particular choice of these parameters. For example, in the case of Cu three- and five-layer films, variation in the $E_{l=2}$ parameter (the most sensitive parameter in d-band films) by about ±0.2 Ry causes eigenvalues to shift by only 1–2 mRy.

3. *Exterior or vacuum region*

The basis function in region III of Fig. 1 is defined as a product of a two-dimensional plane-wave and a z-dependent function and its energy derivative:

$$\varphi^{(i)}_{m,n}(\vec{k},\vec{r}) = [A^{(i)}_{m,n}\, u_{\vec{k},m}(E_v,z) + B^{(i)}_{m,n}\, \dot{u}_{\vec{k},m}(E_v,z)] \times \exp[i(\vec{k}+\vec{g}_m)\cdot\vec{r}]\,, \tag{4a}$$

where $i=1,2$, respectively, for the upper or lower vacuum region and $u_{\vec{k},m}(E_v,z)$ is a solution of the one-dimensional SE in region III with the z-dependent potential, $V(z)$,

$$\left(-\frac{\partial^2}{\partial z^2} + V(z) - (E_v - K_m^2)\right) u_{\vec{k},m}(E_v,z) = 0\,. \tag{4b}$$

The $A_{m,n}$ and $B_{m,n}$ coefficients are determined by matching onto Eq. (1) so that the basis functions and its derivative are continuous across the boundary planes at $z=\pm\frac{1}{2}D$ (cf. Appendix). As stated, the final results are found to be very insensitive to the particular choice of the vacuum constant energy parameter E_v.

B. Secular equations

As defined above, the basis functions are everywhere continuous and differentiable, and the Rayleigh-Ritz variational principle is then easily applied. Expanding the electronic wave function in this basis,

$$\Psi_{\vec{k}}(r) = \sum_{m,n} c_{m,n}(\vec{k})\varphi_{m,n}(\vec{k},\vec{r})\,, \tag{5}$$

and applying the variational principle then yields the secular equations (cf. Appendix),

$$\sum_{m,n} [H_{m'n',mn} - E(\vec{k})O_{m'n',mn}]c_{mn} = 0\,. \tag{6}$$

The Hamiltonian matrix here consists of three terms,

$$H = H_{\mathrm{FMT}} + \Delta H_{I,V} + \Delta H_{\mathrm{NS}}\,, \tag{7}$$

where H_{FMT} is due to the FMT potential, $\Delta H_{I,V}$ is due to the non-FMT correction potential in the interstitial region and in the vacuum region, and ΔH_{NS} is due to the nonspherical (NS) correction inside the MT spheres.

The most important feature of the LAPW secular equations in Eq. (6) is that the Hamiltonian and overlap matrices are energy independent. This permits the simultaneous determination of the eigenvalues and eigenvectors and represents a considerable savings of time and effort.

III. APPLICATIONS

Since our primary aim is to test the method and to demonstrate the wide range of its applicability, the calculations were performed in the non-self-consistent FMT approximation. The film potentials were constructed by overlapping atomic Coulomb potentials and using the local density approximation[26] to obtain the exchange-correlation potential from overlapping atomic charge densities. Self-consistent nonrelativistic atomic wave functions were obtained using a Herman-Skillman type program. Except where otherwise indicated, the exchange-correlation potential was computed using the value $\alpha=\frac{2}{3}$. The resulting potential was spherically averaged inside the MT spheres, volume averaged in the interstitial region and planar averaged in the exterior region.

A. Transition metals

We present here results [all for the (001) surface] for one-, three-, and five-layer fcc Cu films, and for five-layer films of bcc Fe and of fcc Co and Ni. The band structure of the Cu monolayer along lines of symmetry in the two-dimensional Brillouin zone (BZ) is shown in Fig. 2. The two-dimensional BZ for the (001) surface is pictured in the insert. The solid and dashed lines represent, respectively, states which are symmetric and antisymmetric with respect to z reflection. Symmetries are labeled following Ref. 7. Milli-Rydberg convergence was obtained using about 50 basic functions for each symmetry type. For thicker films ~30 basis functions per atom were sufficient to obtain similar convergence. As noted in Sec. II, the $E_{l=2}$ parameter is the most sensitive one in the case of Cu films (variations of about 1 Ry in the others has

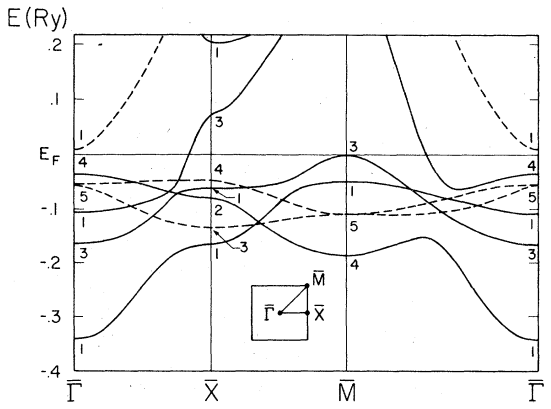

FIG. 2. Band structure for the Cu monolayer. Solid and dashed lines represent bands which are, respectively, symmetric and anti-symmetric with respect to z reflection. The two-dimensional Brillouin zone for the (001) fcc and bcc surface is shown in the insert.

essentially no influence on the total results). For the monolayer $E_{l=2}$ was set equal to 0.31 Ry above the constant interstitial potential. The band structure in Fig. 2 is in good general agreement with other theoretical calculations.[9,11,13,19,24] There are no d holes[9,18] in Fig. 2; the Fermi energy E_F barely cuts above the $\bar{M}_3$ symmetry point. This feature, however, is particularly sensitive to the potential.

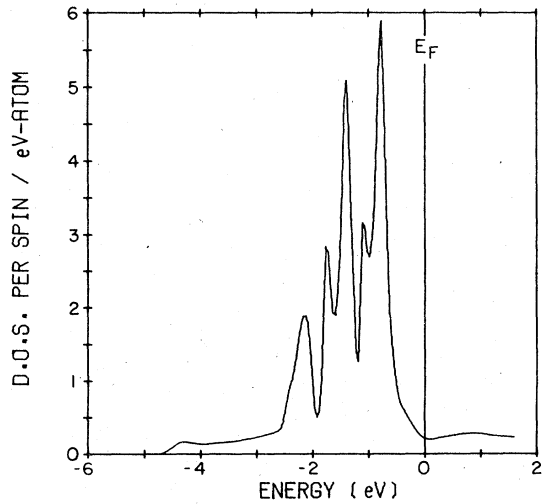

FIG. 3. Density of states for the Cu monolayer.

Wang and Freeman[19] have very recently shown that such d holes (located in a pocket centered at $\bar{M}_3$) disappear on going to self-consistency. We return to this point below.

The density of states (DOS) for the monolayer film is shown in Fig. 3. We have used a two-dimensional generalization[19,24] of the bulk linear analytic tetrahedron method.[32] The DOS was obtained using 15 $\vec{k}$ points in the irreducible $\frac{1}{8}$ of the two-dimensional BZ and then smoothed with a Gaussian (FWHM = 0.1 eV) to suppress noise. Compared to the DOS in bulk Cu, the d-band width has been reduced by about 30%–40%. This narrowing of the d-band is in good agreement with other calculations.

Changes in width have also been observed[33] in angle-resolved photoemission spectra taken at grazing angles in Cu. Mehta and Fadley[34] have shown that this is directly related to the variation in d-band width of the local DOS in the outermost layers. This behavior can be qualitatively seen in Fig. 4, where we show the DOS for one-, three-, and five-layer Cu films. In this figure the d-band width substantially increases on going from the monolayer to the three-layer films, but increases

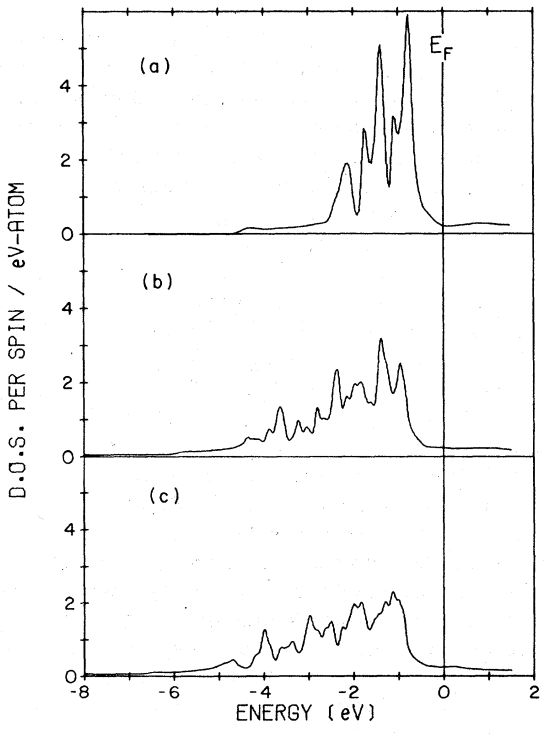

FIG. 4. Density of states for the Cu (a) monolayer, (b) three-layer film, and (c) five-layer film.

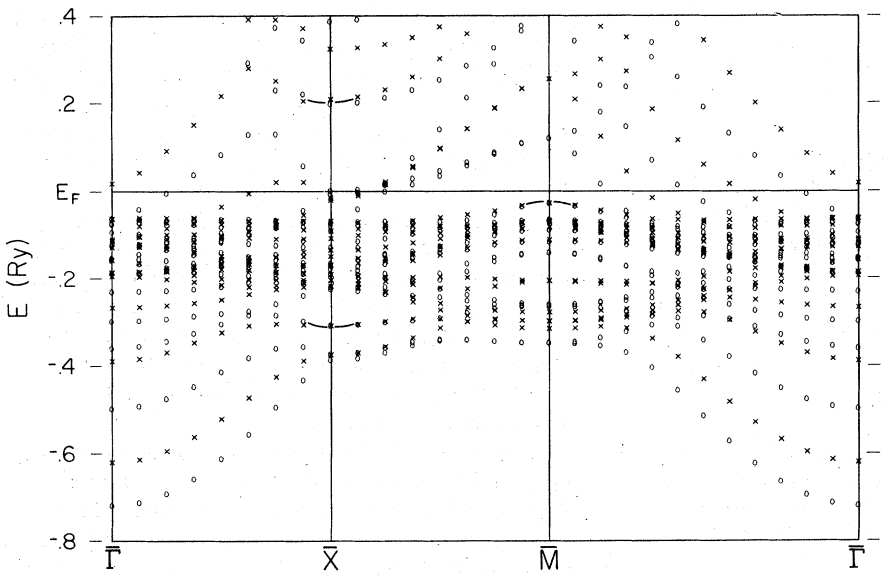

FIG. 5. Band structure for the Cu five-layer film. The circles and crosses represent states which are, respectively, symmetric and anti-symmetric with respect to z reflection. Two surface states at $\bar{X}$ and one at $\bar{M}$ are identified by curved lines.

only slightly on going from three to five layers. This indicates that the d-band width of the second layer local DOS is already becoming close to that of the bulk DOS.

The band structure for the five-layer film is shown in Fig. 5. For the five-layer film, $E_{l=2}$ was set equal to 0.47 Ry. The circles and crosses indicate states which are, respectively, symmetric and antisymmetric with respect to z reflection. Our results are generally in good agreement with the parametrized tight-binding calculation of the energy bands of a 33-layer Cu film of Sohn *et al.*[35] In Fig. 5 we identify SS occurring in absolute band gaps by curved lines. There are two at $\bar{X}$, an occupied state at ~−0.3 Ry and an unoccupied one at ~0.2 Ry. These SS were also found in Ref. 35. The SS at $\bar{M}$ near E_F was not found, however, in Ref. 35. We have also found this SS at $\bar{M}$ in Co and Ni (discussed below).

The DOS for our three- and five-layer Cu films are compared to the bulk DOS in Fig. 6. All curves have been smoothed with a Gaussian of FWHM = 0.1 eV. The bulk band structure is a non-MT, self-consistent LAPW calculation[36] using the same exchange-correlation parameter, $\alpha = \frac{2}{3}$. While there is rough agreement with respect to shape and width, the d-band width of the five-layer film is greater than in bulk, and the distance between the d-band edge and E_F is smaller by about 0.6 eV in the film results than in bulk.[37] Possible explanations for these discrepancies include: (i) the neg-

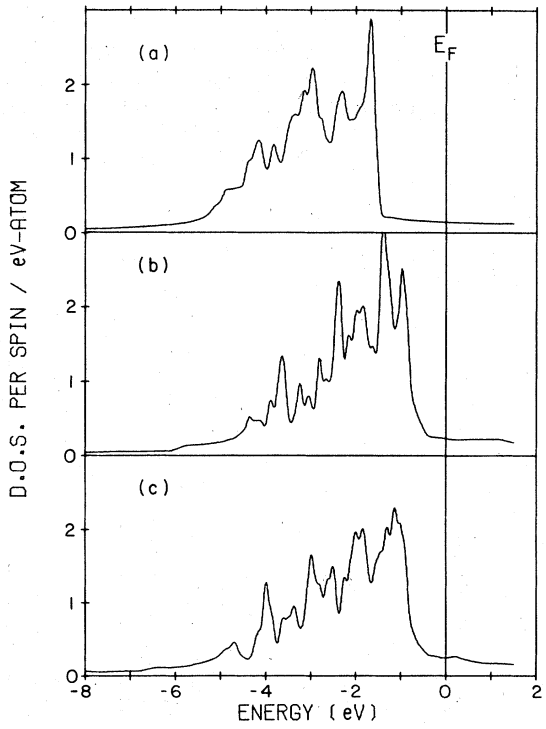

FIG. 6. Density of states for (a) bulk Cu (Ref. 36), (b) the three-layer Cu film, and (c) the five-layer Cu film.

lect of non-FMT contributions to the potential, (ii) size effects which would become smaller on going to thicker films, and (iii) the use of a non-self-consistent potential.

Regarding (i), the potential in the five-layer film interstitial region varies over a range of about 0.8 Ry with the average value falling near the middle of this range (this is also true for the Fe, Co, and Ni films). Nonspherical potential terms inside the MT spheres and x-y dependent terms in the vacuum region are both substantially smaller, so that we focus attention on the nonconstant terms in the interstitial region. While these terms are large indeed, one would expect that the neglect of these terms would lead to an overall *narrowing* of the d bands and a *downward* shift of the d bands relative to the sp bands. This is because the volume average of the interstitial potential in the atomic Wigner-Seitz cell of a central plane atom is *lower* in energy than the total film average taken over all layers. The use of the total film average in the FMT potential should, therefore, introduce a relative narrowing in the central plane DOS compared to, for example, a warped-MT calculation. We have, in fact, observed an indication of this behavior (discussed below) in a calculation employing an exchange parameter $\alpha = 1$.

Size effects (ii) can manifest themselves in the following way. We find that the overall sp-band width in the five-layer Cu film is about 0.1 Ry smaller than in bulk. Similar behavior was found by Wang and Freeman[20] in a self-consistent LCAO calculation for a five-layer (001) Ni film. They found that the overall sp-band width was about 0.05 Ry smaller than in bulk, although the d-band width was essentially the same as in bulk. In addition, they found a lowering (by about 0.05 Ry) of the film-derived Γ_1 state relative to the bulk value of Γ_1. Since E_F falls inside the d bands in Ni, such size effects do not significantly affect the location of E_F. By contrast, this behavior in Cu could contribute to the relative position of E_F and the d-band edge, although it does not account for the difference in d-band width between the five-layer film and bulk.

The third possibility (iii) is supported by results obtained by Wang and Freeman[19] in a self-consistent LCAO calculation for a Cu monolayer. They find that on going to self-consistency the d band is narrowed by 0.16 eV and its center of gravity is lowered by approximately 0.4 eV with respect to E_F. As noted, this causes the d holes in their non-self-consistent calculation to disappear. In non-self-consistent bulk calculations for d-band metals, the use of a variable exchange-correlation parameter α (with α taking a value near or equal to 1) leads to results (at least for the eigenvalues) which

TABLE I. Comparison of LAPW results for the Cu monolayer with the self-consistent (SC) results of Ref. 19 (energies in eV).

	Non-SC (19) $\alpha=\frac{2}{3}$	LAPW $\alpha=\frac{2}{3}$	LAPW $\alpha=0.722$	SC (19) $\alpha=\frac{2}{3}$
E_F	−3.74	−3.82	−4.23	−4.92
$E_F-\bar{M}_3$	−0.18	0.02	0.31	0.29
$\bar{M}_3-\bar{M}_4$	2.71	2.52	2.39	2.55
$E_F-\bar{\Gamma}_1$	5.16	4.68	4.58	4.85

are close to those obtained self-consistently[38] with $\alpha=\frac{2}{3}$. Thus one can try to simulate the effects of self-consistency on the film band structure by varying α. We found for the Cu monolayer, that a value of $\alpha=0.72$ more closely approximates (Table I) the self-consistent results of Wang and Freeman.[19] The effect of a similar variation of α for the five-layer film is shown in Fig. 7 which pre-

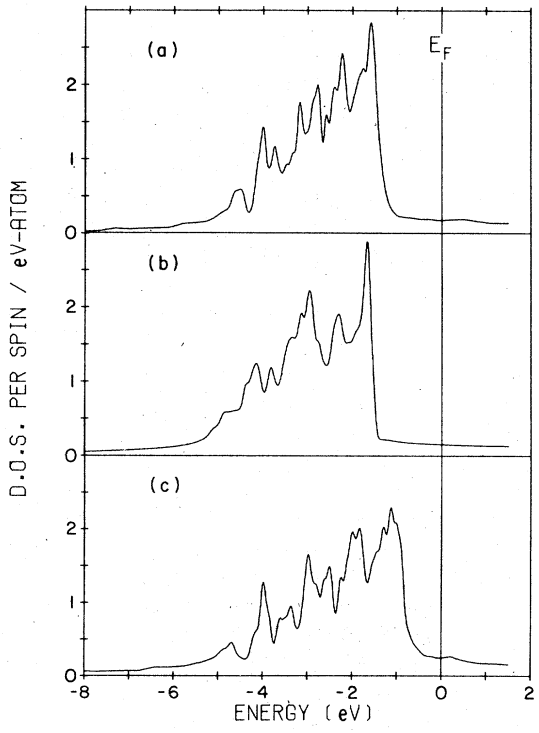

FIG. 7. Density of states for (a) five-layer Cu film with $\alpha=0.82$, (b) bulk Cu (Ref. 36), and (c) the five-layer Cu film with $\alpha=\frac{2}{3}$ [same as Fig. 6(c)].

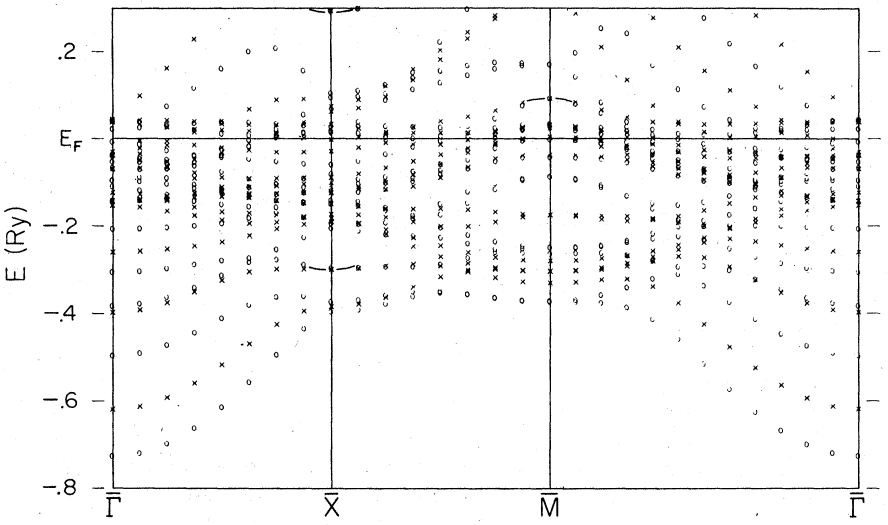

FIG. 8. Band structure for the Co five-layer film. Two surface states at $\bar{X}$ and one at $\bar{M}$ are identified by curved lines.

sents several of the same curves as in Fig. 6 except that the film DOS has been computed using $\alpha = 0.82$ to achieve better agreement with the bulk results. All the SS identified in Fig. 5 remain in the $\alpha = 0.82$ calculation. The agreement between Fig. 7(a) ($\alpha = 0.82$) and Fig. 7(b) (bulk) is remarkably good. This is somewhat surprising at first, since Wang and Freeman[20] found that their total DOS for a five-layer Ni (001) film differs substantially from the bulk DOS, although their central plane DOS closely resembles the bulk results. They attribute this to the fact that their surface plane DOS is substantially more narrow than their central plane DOS. The d-band width is greater in Ni than in Cu, however, and it is possible that the broader Ni d band suffers more severe narrowing (compared to Cu) on the surface-plane relative to the central plane. While we have not calculated planar DOS's, this behavior seems to occur for Cu in Ref. 35; compare with Ref. 20 and Ref. 39 for Ni.

A calculation for a five-layer Cu film using $\alpha = 1$ resulted in a d band which was narrowed by about 1 eV compared to the bulk result with the distance between E_F and the d-band edge equal to about 2.5 eV. While non-self-consistent bulk calculations with $\alpha = 1$ generally yield good agreement with bulk self-consistent calculations with $\alpha = \frac{2}{3}$, this behavior for the five-layer film with $\alpha = 1$ confirms the expectations discussed above concerning the neglect of the nonconstant potential terms in the film interstitial region. The successful use of $\alpha = 0.82$ suggests that this intermediate value represents a trade-off between (i) compensating, to a degree,

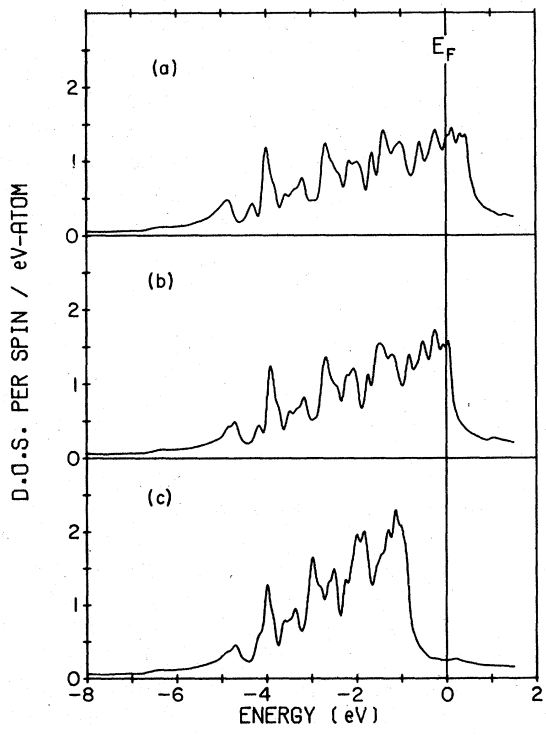

FIG. 9. Density of states for five-layer films of (a) Co, (b) Ni, and (c) Cu.

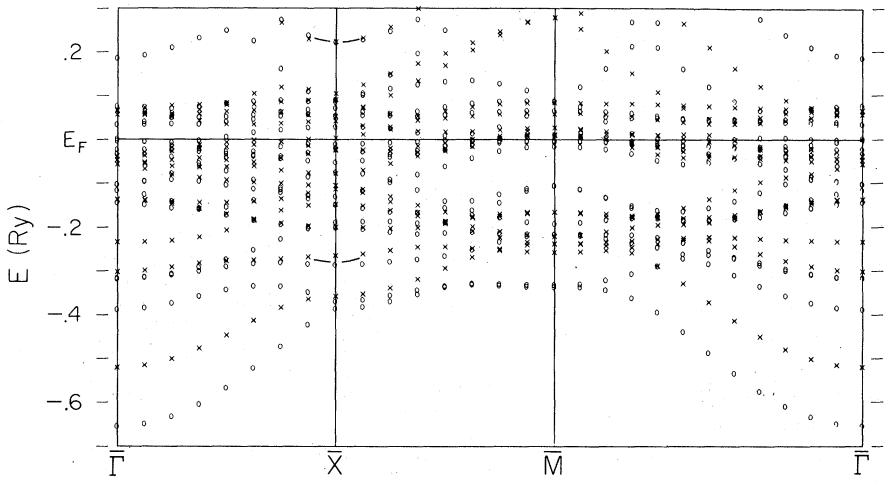

FIG. 10. Band structure for the bcc Fe five-layer film. Two surface states at $\bar{X}$ are identified by curved lines.

for the neglect of the nonconstant potential, and (ii) simulating self-consistency. We believe, therefore, that in a warped-MT calculation, the use of an exchange parameter nearer $\alpha = 1$ would more closely agree with the bulk self-consistent results. A similar trade-off may be present for the Cu monolayer. In this connection, it is interesting to note that in Ref. 24 a Cu-monolayer calculation using a *bulk* MT-potential with $\alpha = 1$ yields results in generally good agreement with our $\alpha = \frac{2}{3}$ Cu monolayer band structure.

Keeping in mind the characteristics of the $\alpha = \frac{2}{3}$ FMT calculations discussed above, we now present our results for Co, Ni, and Fe. In Fig. 8 we show the band structure for a five-layer fcc Co film. Here we have identified three SS which are the counterparts of those shown in Fig. 5 for Cu (the upper SS at $\bar{X}$ in Fig. 8 is just below vacuum). We also find these SS in the five-layer Ni bands. The SS at $\bar{M}$ in Cu (Fig. 5) was not found in Ref. 35, but this state was found in the ferromagnetic Ni bands of Ref. 40. In the majority spin bands of Ref. 40, this state belongs to a band of SS which was used to account for the reversal of photoelectron-spin polarization just above threshold.

Figure 9 compares the total DOS for five-layer films of fcc Co, Ni, and Cu (all calculated with $\alpha = \frac{2}{3}$). With regard to such general features as d-band width and the location of E_F, these results show trends which are similar to those in bulk.

In Fig. 10 we show the band structure for a five-layer bcc-Fe film. General features of the energy bands are in good agreement with the supplemented OPW calculation of Caruthers *et al.*[8] We identify at $\bar{X}$ two clear examples of SS occurring in absolute bulk energy gaps. These were also found in Ref. 8. In Fig. 11 we show the DOS of the five-layer Fe film. This DOS has the characteristic signature of the bcc structure and is in good agreement with Ref. 8.

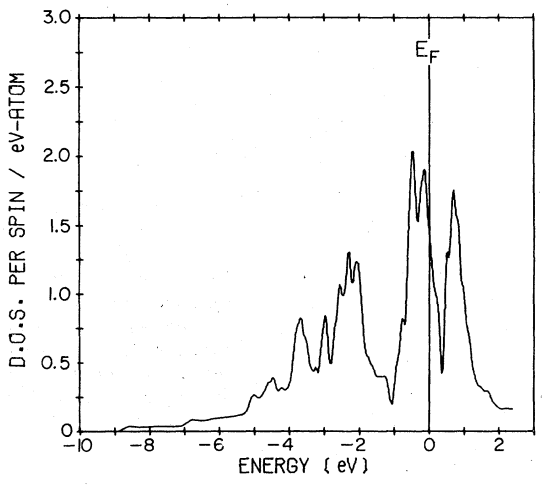

FIG. 11. Density of states for the five-layer Fe film.

B. Aluminum

For NFE-like crystals the number of basis functions required for convergence is much less than in d-band metals. In Fig. 12 we show the band structure along the symmetry line $\bar{\Gamma}$-$\bar{X}$ for a nine-layer Al (001) film. In this calculation 110 basis functions were used to obtain convergence to about 10 mRy. As before, plus and minus signs in this figure label states which are, respectively, symmetric and antisymmetric with respect to z reflection. All the bands shown in Fig. 12 have the same two-dimensional $\bar{\Delta}_1$ symmetry, so that the only allowed crossings are between states of different z-reflection symmetry. The "oscillatory" behavior is thus due to anticrossings of bands with the same two-dimensional symmetry. Upon going to the limit of an infinitely thick film, the anticrossings will look more and more like true crossings, and the bands will look more and more like NFE parabolas.

This can be seen from consideration of the band structure in this limit, i.e., the bulk projected bands, shown in Fig. 13 (taken from Ref. 31). Because all the bands in Fig. 13 have the same $\bar{\Delta}_1$ symmetry, bands with the same value of k_z (the z component of the three-dimensional Bloch momentum) must repel one another, thus causing the bulk energy gaps shown. Bands with different values of k_z may cross, however, since k_z is a good quantum number in the bulk.

In a film, by contrast, there is no periodicity in the z direction, and k_z is no longer a good quantum number. Thus crossings of bulk bands with different values of k_z must become anticrossings in the film calculation. As the film becomes thicker, however, k_z is more and more nearly a good quantum number, and the anticrossings begin to look more like true crossings. In the light of these remarks, one can see the close similarity of our nine-layer film bands (Fig. 12) and the bulk projected bands (Fig. 13).

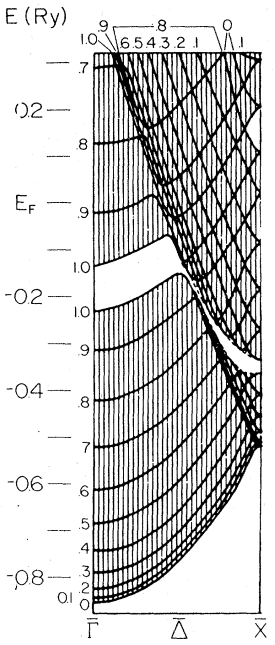

FIG. 13. Projected bulk bands for Al (001) along $\bar{\Gamma}$–$\bar{X}$ (Ref. 31). The numbers which label the bands represent values of k_z in units of $2\pi/A$, where A is the bulk lattice parameter.

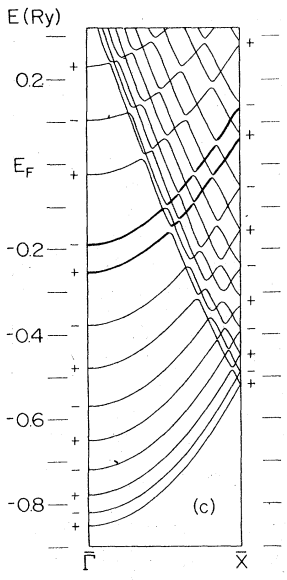

FIG. 12. Band structure for the nine-layer Al film along $\bar{\Gamma}-\bar{X}$. A pair of surface states are identified by heavy lines. The (+) and (–) signs denote states which are, respectively, symmetric and anti-symmetric with respect to z reflection.

C. Surface and resonance states in Al (001)

This similarity (particularly with regard to the NFE-like behavior which emerges from the extreme anticrossings in our bands) is crucial to understanding a very recent photoemission measurement by Gartland and Slagsvold[29] of an occupied SS *and* resonance on clean Al (001). We identify the relevant pair of SS by heavy lines in Fig. 12. These SS states run from $\bar{\Gamma}$ to about one-half the distance to $\bar{X}$. They then persist as a resonance into the region of bulk continuum states. Note that the resonance "hops" across different film energy bands following a free-electron-like dispersion. The SS has previously been found in Refs. 30 and 31, but the existence of the surface resonance was first reported by us.[28] Gartland and Slagsvold[29] have identified this SS in their angular resolved photoemission spectra. They found a parabolic dispersion relation which starts in the bulk band gap at

TABLE II. Comparison of the experimental and theoretical (nine-layer film) surface state–surface resonance (SS-SR) for Al (001) along $\bar{\Gamma}-\bar{X}$ (energies in eV).

	(–) SS-SR	(+) SS-SR	Average	Expt. (Ref. 29)
$E_F - E_{SS}(\bar{\Gamma})$	2.53	3.41	2.97	2.80 ± 0.2
m^*/m	1.04 ± 0.03	1.04 ± 0.03	1.04	1.03 ± 0.1

$\bar{\Gamma}$ and continues smoothly up in the band gap through the continuum region [which starts in Fig. 13 at $\vec{k}_{\parallel} = (0.5, 0)$ in units of π/a, where a is the surface lattice parameter] to E_F. Up to $k_{\parallel} = 0.5$ the measured dispersion relation agrees well with all the film calculations. At larger values of $k_{\parallel}$, however, these authors were not able to correlate the observed peak behavior with the existing surface state calculations.[30,31] By contrast, the experimental dispersion relation agrees extremely well with the heavy curves in our band structure in Fig. 12. The comparison is summarized in Table II. The average values listed in Table II are probably reliable indicators of the limiting values as the film gets thicker and thicker (and the energy splitting between the SS approaches zero), and the agreement with experiment is remarkably good here. The experiment, which is sensitive to states localized at the surface, thus detects a true SS for $k_{\parallel} \leq 0.5$ and a surface resonance for large $k_{\parallel}$.[41] Inspection of previous surface calculations for Al shows no hint of this essentially free-electron-like behavior, which is evident in our results because of the extreme anticrossing behavior of our bands. Theoretically, the observed transition from a true SS to a surface resonance is explained[28] in terms of a mechanism in NFE metals for the formation of surfair resonance states in "partial" Bragg reflection energy gaps. This and a more complete discussion of the SS resonance is presented in Ref. 28.

ACKNOWLEDGMENTS

We thank D. E. Ellis, W. Pickett, and C. P. Wang for helpful discussions. We are especially grateful to D. D. Koelling for making available his bulk LAPW programs and for his helpful discussions and collaboration. The work reported here was supported by the NSF under Grant No. DMR 77-23776 and the U. S. Department of Energy. One of us (M.P.) acknowledges the support of the Swiss National Science Foundation.

APPENDIX: DETAILS OF THE FILM LAPW FORMALISM

A. Identities for the relativistic radial functions inside the MT spheres

The radial function $u_{l,\alpha}(E_l, r)$ is taken to be the large component radial function of the solution of the Dirac equation in the limit of zero spin-orbit coupling. In this limit, we follow the formulation of Koelling and Harmon[27] for solving the Dirac equation and obtain solutions for a coupled pair of linear differential equations exactly as in Ref. 27. For the purpose of deriving some useful identities, however, it is convenient to replace this coupled set of equations by a (completely equivalent) single Pauli-like equation:

$$\frac{1}{r}\frac{\partial^2(ru)}{dr^2} - \frac{l(l+1)u}{r^2} + 2m(E-V)u + h_R u = 0\,, \tag{A.1}$$

where the relativistic correction terms are contained in h_R,

$$h_R \equiv \left(\frac{V'}{2Mc^2}\frac{\partial}{\partial r} + \frac{(E-V)^2}{c^2}\right), \tag{A.2}$$

and $M \equiv m + (1/2c^2)(E-V)$. Differentiating (A.1) with respect to energy yields a differential equation for the radial energy derivative function $\dot{u}_{l,\alpha}(E_l, r)$,

$$\frac{1}{r}\frac{\partial^2(r\dot{u})}{\partial r^2} - \frac{l(l+1)\dot{u}}{r^2} + 2m(E-V)\dot{u} + h_R\dot{u} = -2mu - \dot{h}_R u\,. \tag{A.3}$$

If the functions $u_{l,\alpha}$ are first normalized inside the MT spheres as

$$\int_0^{R_\alpha} r^2 u_{l,\alpha}\, dr = 1\,, \tag{A.4}$$

then $u_{l,\alpha}$ and $\dot{u}_{l,\alpha}$ will be orthogonal [as can be seen by differentiating (A.4) with respect to energy]. Multiplying (A.1) by $r^2\dot{u}_l$ and (A.2) by $r^2 u_l$, subtracting (A.2) from (A.1), and integrating $\int_0^{R_\alpha} dr$ then yields the identity

$$R_\alpha^2\left(\dot{u}\frac{\partial}{\partial r}u - u\frac{\partial}{\partial r}\dot{u}\right)_{R_\alpha} = 2m + \int_0^{R_\alpha}\left[\frac{\partial}{\partial E}\left(\frac{V' u^{-1}(\partial u/\partial r)}{2Mc^2} + \frac{(E-V)^2}{c^2}\right)\right] u^2 r^2\, dr\,, \tag{A.5}$$

where we have used (A.4). In obtaining (A.5) we have neglected terms in the integrand proportional to $\partial M/\partial E$, since these are smaller by a factor of $1/c^2$.

The integral appearing in (A.5) is essentially the expectation value of the *energy derivative* of the relativistic corrections, h_R. This term is extremely small, and an excellent approximation to (A.5) is the identity (in Rydberg a.u.):

$$R_\alpha^2\left(\dot{u}\frac{\partial}{\partial r}u - u\frac{\partial}{\partial r}\dot{u}\right)_{R_\alpha} = 1\,. \tag{A.6}$$

B. Identities for the z-dependent functions in the vacuum regions

A relation similar to Eq. (A.6) can be obtained for $u_{\vec{k},m}(E_v, z)$ and its energy derivative, $\dot{u}_{\vec{k},m}(E_v, z)$. $u_{\vec{k},m}$ is first normalized as

$$\int_{\frac{1}{2}D}^{\infty} u_{\vec{k}m}^2\, dz = 1 \tag{A.7}$$

to insure the orthogonality of $u_{\vec{k},m}$ and $\dot{u}_{\vec{k},m}$. A differential equation for $\dot{u}_{\vec{k},m}$ is then obtained from the SE for $u_{\vec{k},m}$ [cf. Eq. (4b) in the text]. Repeating essentially the same steps described above then yields the identity

$$\left(\dot{u}_{\vec{k},m}\frac{\partial}{\partial z}u_{\vec{k},m} - u_{\vec{k},m}\frac{\partial}{\partial z}\dot{u}_{\vec{k},m}\right)_{z=D/2} = -1\,. \tag{A.8}$$

C. Expansion coefficients

Using the relation (A.6), expressions for the expansion coefficients $A_{L,\alpha}$ and $B_{L,\alpha}$ can be obtained by matching Eq. (3) onto the symmetrized plane-wave basis function and requiring that each angular momentum term be continuous with a continuous derivative:

$$A_{L,\alpha}^{\pm} = 4\pi R_\alpha^2 \Omega^{-1/2} e^{i\vec{K}_m\cdot\vec{\gamma}_\alpha} a_{l,\alpha}(m,n) Y_{L,\alpha}^{\pm}(m,n)\,, \tag{A.9a}$$

$$B_{L,\alpha}^{\pm} = 4\pi R_\alpha^2 \Omega^{-1/2} e^{i\vec{K}_m\cdot\vec{\gamma}_\alpha} b_{l,\alpha}(m,n) Y_{L,\alpha}^{\pm}(m,n)\,, \tag{A.9b}$$

where

$$Y_{L,\alpha}^{\pm}(m,n) \equiv 2^{-1/2}\left[e^{ik_n\gamma_{\alpha z}} Y_L(\vec{K}_m + \vec{k}_n) \pm e^{-ik_n\gamma_{\alpha z}} Y_L(\vec{K}_m - \vec{k}_n)\right] \tag{A.9c}$$

and

$$a_{l,\alpha}(m,n) \equiv \left[j_l'(G_{mn}R_\alpha)\,\dot{u}_{l,\alpha} - j_l(G_{mn}R_\alpha)\,\dot{u}_{l,\alpha}'\right], \tag{A.9d}$$

$$b_{l,\alpha}(m,n) \equiv \left[j_l(G_{mn}R_\alpha)\,u_{l,\alpha}' - j_l'(G_{mn}R_\alpha)\,u_{l,\alpha}\right]. \tag{A.9e}$$

Here $\vec{\gamma}_\alpha$ is the position vector of the αth atom in the unit cell,

$\vec{K}_m \equiv \vec{k} + \vec{g}_m$, $\vec{k}_n \equiv k_n \hat{z}$, and $G_{mn} \equiv |\vec{K}_m + \vec{k}_n| = |\vec{K}_n - \vec{k}_n|$.

The (+) and (−) denote states which are, respectively, symmetric and antisymmetric with respect to z reflection. In Eqs. (A.9a) and (A.9b) there is no denominator which can vanish, thus eliminating the asympote problem of the conventional APW method [actually the "denominator" is $(\dot{u}u' - u\dot{u}')$, which is simply replaced, from (A.6) by $1/R_\alpha^2$].

Similarly, using Eq. (A.8), expressions for the expansion coefficients $A_{m,n}^{(i)}$ and $B_{m,n}^{(i)}$ can be obtained by matching Eq. (4) onto the symmetrized plane wave at $z = \pm\frac{1}{2}D$. For the upper-boundary plane ($z = \frac{1}{2}D$) we have:

$$A_{m,n}^{(1)\pm} = (2/\Omega)^{1/2}(-1)^n \dot{u}_{\vec{k},m}^{\ell}(\tfrac{1}{2}D)\,, \tag{A.10a}$$

$$B_{m,n}^{(1)\pm} = -(2/\Omega)^{1/2}(-1)^n u_{\vec{k},m}^{\ell}(\tfrac{1}{2}D)\,. \tag{A.10b}$$

Note that, formally, Eqs. (A.10a) and (A.10b) are valid for both (+) and (−) symmetry types, although the index n refers to different definitions of k_n^+ and k_n^- (Eq. 2). The expansion coefficients on the lower-boundary plane ($z = -\frac{1}{2}D$) are simply related (by symmetry) to those at the upper plane:

$$A_{m,n}^{(2)\pm} = \pm A_{m,n}^{(1)}\,, \tag{A.10c}$$

$$B_{m,n}^{(2)\pm} = \pm B_{m,n}^{(1)}\,. \tag{A.10d}$$

D. Hamiltonian and overlap matrices

The overlap matrix is given by

$$O_{m'n',mn}^{\pm} = \langle\varphi_{m'n'}^{\pm}(\vec{k},\vec{r})\,|\,\varphi_{mn}^{\pm}(\vec{k},\vec{r})\rangle = U_{m'n',mn}^{\pm} + \frac{4\pi}{\Omega}\sum_\alpha \exp[-i(\vec{g}_m - \vec{g}_{m'})\cdot\vec{\gamma}_\alpha] \times R_\alpha^4 \sum_l (2l+1) S_{l\alpha} P_{l\alpha}^{\pm} + S_{m'n',mn}\,. \tag{A.11a}$$

The first two terms come from inside the boundary

planes, $|z| \leq \frac{1}{2}D$: the first term is the contribution from the interstitial region, and the second term is the contribution from all the MT spheres. The third term in (A.11a) comes from the exterior or vacuum regions, $|z| \geq \frac{1}{2}D$. The quantities in Eq. (A.11a) are defined as follows:

$$U^{\pm}_{m'n',mn} \equiv \delta_{m'n',mn}\epsilon^{\pm}_{n} - \frac{4\pi}{\Omega}\sum_{\alpha}\exp[-i(\vec{g}_m - \vec{g}_{m'})\cdot\vec{\gamma}_\alpha]R^2_\alpha\{\cos[(k_n - k_{n'})\gamma_{\alpha z}]J_\alpha(\vec{G}^{+}_{m'n'},\vec{G}^{+}_{mn}) \pm \cos[(k_n + k_{n'})\gamma_{\alpha,z}]J_\alpha(\vec{G}^{+}_{m'n'},\vec{G}^{-}_{mn})\}\,, \tag{A.11b}$$

$$S_{l,\alpha} \equiv a_{l,\alpha}(m'n')a_{l,\alpha}(mn) + b_{l,\alpha}(m'n')b_{l,\alpha}(mn)N_{l,\alpha}\,, \tag{A.11c}$$

$$P^{\pm}_{l,\alpha} \equiv \{\cos[(k_n - k_{n'})\gamma_{\alpha z}]P_l(\hat{G}^{+}_{m'n'}\cdot\hat{G}^{+}_{mn}) \pm \cos[k_n + k_{n'})\gamma_{\alpha z}]P_l(\hat{G}^{+}_{m'n'}\cdot\hat{G}^{-}_{mn})\}, \tag{A.11d}$$

$$S_{m'n',mn} \equiv 2\,\delta_{m'm}A\,[A^{(1)}_{mn}A^{(1)}_{mn'} + B^{(1)}_{mn}B^{(1)}_{mn'}N_m], \tag{A.11e}$$

with

$$J_\alpha(\vec{x},\vec{y}) \equiv j_1(|\vec{x}-\vec{y}|R_\alpha)/|\vec{x}-\vec{y}|\,. \tag{A.11f}$$

Here

$$\epsilon^{-}_{n} \equiv 1,\quad \epsilon^{+}_{n} \equiv (1+\delta_{n,0}),\quad N_{l,\alpha} \equiv \int_0^{R_\alpha} \dot{u}^2_{l,\alpha}r^2\,dr\,,$$
$$\vec{G}^{\pm}_{mn} \equiv \vec{K}_m \pm k_n\hat{z}\,,$$

$P_l(\hat{r}_1\cdot\hat{r}_2)$ is a Legendre polynomial,

$$N_m \equiv \int_{\frac{1}{2}D}^{\infty} \dot{u}^2_{k,m}(z)\,dz\,,$$

and A is the cross-sectional area of the unit cell.

The Hamiltonian matrix is given as the sum of three terms (Eq. 7):

$$H^{\pm}_{m'n'} = H_{\mathrm{FMT}} + \Delta H_{I,V} + \Delta H_{\mathrm{NS}} = \langle\varphi^{\pm}_{m'n'}|H_{\mathrm{FMT}}\,|\varphi^{\pm}_{mn}\rangle + \langle\varphi^{\pm}_{m'n'}|\Delta V_{I,V}\,|\varphi^{\pm}_{mn}\rangle_{\mathrm{II,III}} + \langle\varphi^{\pm}_{m'n'}|\Delta V_{\mathrm{NS}}\,|\varphi^{\pm}_{mn}\rangle_{\mathrm{I}}\,,$$

where $\Delta_{I,V}$ is the correction potential in the interstitial and vacuum regions (II and III in Fig. 1) and ΔV_{NS} is the nonspherical correction potential in the MT spheres (I in Fig. 1). We present here expressions for H_{FMT}.

$$H^{\pm\mathrm{FMT}}_{m'n',mn} = G^2_{m'n'}U^{\pm}_{m'n',mn} + \frac{4\pi}{\Omega}\sum_{\alpha}\exp[-i(\vec{g}_m - \vec{g}_{m'})\cdot\vec{\gamma}_\alpha]R^4_\alpha\sum_l(2l+1)[E_l S_{l,\alpha} + a_{l,\alpha}b_{l,\alpha}]P^{\pm}_{l,\alpha} + E_V S_{m'n',mn} + 2\delta_{m'm}AA^{(1)}_{mn}B^{(1)}_{mn'}\,. \tag{A.12}$$

Here, the E_l are the constant-energy parameters inside the MT spheres, and E_v is the constant-energy parameter for the vacuum regions. Individually, the first two terms are not Hermitian [the fourth term is Hermitian, as can be seen by inspection of Eqs. (A.10a) and (A.10b)]. The non-Hermitian parts can be combined, however, to yield an expression which is manifestly Hermitian, for the first two terms. This is done using a standard identity[42] for a Bessel function summation occurring in these terms. The resulting Hermitian expression for the first two terms of Eq. (A.12) is:

$$G^2_{m'n'}\delta_{m'n',mn}\epsilon_{n\pm} - \frac{4\pi}{\Omega}\sum_{\alpha}\exp[-i(\vec{g}_m - \vec{g}_{m'})\cdot\vec{\gamma}_\alpha]R^2_\alpha\{\cos[(k_n - k_{n'})\gamma_{\alpha,z}]J_\alpha(G^+,G^+)(\vec{G}^{+}_{m'n'}\cdot\vec{G}^{+}_{mn}) \pm \cos[(k_n + k_{n'})\gamma_{\alpha,z}]J_\alpha(G^+,G^-)(\vec{G}^{+}_{m'n'}\cdot\vec{G}^{-}_{mn})\} + \frac{4\pi}{\Omega}\sum_{\alpha}\exp[-i(\vec{g}_m - \vec{g}_{m'})\cdot\vec{\gamma}_\alpha]R^4_\alpha\sum_l(2l+1)[E_l S_{l,\alpha} + \gamma_{l,\alpha}]P^{\pm}_{l,\alpha}\,, \tag{A.13a}$$

where

$$\gamma_{l,\alpha} \equiv \dot{u}_{l\alpha}u'_{l\alpha}[j'_l(G_{m'n'}R_\alpha)j_l(G_{mn}R_\alpha) + j_l(G_{m'n'}R_\alpha)j'_l(G_{mn}R_\alpha)] - [\dot{u}'_{l,\alpha}u'_{l,\alpha}j_l(G_{m'n'}R_\alpha)j_l(G_{mn}R_\alpha) + \dot{u}_{l,\alpha}u_{l,\alpha}j'_l(G_{m'n'}R_\alpha)\,j'_l(G_{mn}R_\alpha)]\,. \tag{A.13b}$$

[1]*Photoemission and the Electronic Structure of Surfaces*, edited by B. Feuerbacher, B. Fitton, and R. F. Willis (Wiley, London, 1978).
[2]H. D. Hagstrum, Phys. Rev. 150, 495 (1966).
[3]D. R. Penn and E. W. Plummer, Phys. Rev. B 9, 1216 (1974); P. Soven, E. W. Plummer, and N. Kar, Crit. Rev. Solid State Sci. 6, 111 (1976); N. J. Dionne and T. N. Rhodin, Phys. Rev. B 14, 322 (1976), and references therein.
[4]M. Landolt and M. Campagna, Phys. Rev. Lett. 38, 663 (1977); M. Landolt and Y. Yafet, *ibid.* 40, 1401 (1978).
[5]For a review of theoretical methods up to 1975 see, J. A. Appelbaum and D. R. Hamann, Rev. Mod. Phys. 48, 479 (1976).
[6]J. A. Appelbaum and D. R. Hamann, Phys. Rev. B 6, 2166 (1972).
[7]G. P. Alldredge and L. Kleinman, Phys. Rev. Lett. 28, 1264 (1972).
[8]L. Kleinman and E. B. Caruthers, Phys. Rev. B 10, 3213 (1974); E. B. Caruthers, D. G. Dempsey, and L. Kleinman, *ibid.* 14, 288 (1976).
[9]B. R. Cooper, Phys. Rev. Lett. 30, 1316 (1973).
[10]W. Kohn, Phys. Rev. B 11, 3756 (1975).
[11]N. Kar and P. Soven, Phys. Rev. B 11, 3761 (1975).
[12]R. V. Kasowski, Phys. Rev. B 8, (1976).
[13]G. S. Painter, Phys. Rev. B 17, 3848 (1978).
[14]M. Schlüter, J. R. Chelikowsky, S. G. Louie, and M. L. Cohen, Phys. Rev. Lett. 34, 1385 (1975); S. G. Louie, K.-M. Ho, J. R. Chelikowsky, and M. L. Cohen, Phys. Rev. B 15, 5627 (1977).
[15]S. G. Louie, Phys. Rev. Lett. 40, 1525 (1978).
[16]H. Krakauer and B. R. Cooper, Phys. Rev. B 16, 605 (1977).
[17]J. G. Gay, J. R. Smith, and F. J. Arlinghaus, Phys. Rev. Lett. 38, 561 (1977).
[18]B. R. Cooper, Phys. Rev. B 16, 5595 (1977).
[19]C. S. Wang and A. J. Freeman, Phys. Rev. B 18, 1714 (1978).
[20]C. S. Wang and A. J. Freeman, Phys. Rev. B 19, 793 (1979).
[21]While the method in Refs. 7 and 8 is technically identified as a film or slab method, it can be viewed as a slab-superlattice method with the additional requirement that each plane-wave component must vanish at the midpoint of the vacuum region between neighboring slabs.
[22]H. Krakauer, M. Posternak, and A. J. Freeman, Bull. Am. Phys. 23, 258 (1978); M. Posternak, H. Krakauer, A. J. Freeman, and D. D. Koelling, *ibid.* 23, 259 (1978).
[23]D. D. Koelling and G. O. Arbman, J. Phys. F 5, 2041 (1975); O. K. Andersen, Phys. Rev. B 12, 3060 (1975).
[24]An independently developed version of a similar film LAPW formalism is given in O. Jepsen, J. Madsen, and O. K. Andersen, Phys. Rev. B 18, 605 (1978).
[25]T. Loucks, *Augmented Plane Wave Method* (Benjamin, New York, 1967).
[26]W. Kohn and L. J. Sham, Phys. Rev. 140, A1133 (1965).
[27]D. D. Koelling and B. N. Harmon, J. Phys. C 10, 3107 (1977).
[28]H. Krakauer, M. Posternak, and A. J. Freeman, Phys. Rev. Lett. 41, 1072 (1978).
[29]P. O. Gartland and B. J. Slagsvold, Solid State Commun. 25, 489 (1978).
[30]D. S. Boudreaux, Surf. Sci. 28, 344 (1971).
[31]E. B. Caruthers, L. Kleinman, and G. P. Alldredge, Phys. Rev. B 8, 4570 (1973).
[32]G. Lehman and M. Taut, Phys. Status Solidi 54, 469 (1972); O. Jepsen and O. K. Andersen, Solid State Commun. 9, 1763 (1971).
[33]J. Stohr, G. Apai, P. S. Wehner, F. R. McFeely, R. S. Williams, and D. A. Shirley, Phys. Rev. B 14, 5144 (1976).
[34]M. Mehta and C. S. Fadley, Phys. Rev. Lett. 39, 1569 (1977).
[35]K. S. Sohn, D. G. Dempsey, L. Kleinman, and E. Caruthers, Phys. Rev. B 13, 1515 (1976).
[36]D. D. Koelling (to be published).
[37]This energy difference varies over a range of about 1.5–2.0 eV in bulk calculations. See for example, J. F. Janak, A. R. Williams, and V. L. Moruzzi, Phys. Rev. B 6, 4367 (1972); G. A. Burdick, Phys. Rev. 129, 138 (1963).
[38]J. Callaway and C. S. Wang, Phys. Rev. B 7, 1096 (1973).
[39]D. G. Dempsey, W. R. Grise, and L. Kleinman Phys. Rev. B 18, 1270 (1978).
[40]D. G. Dempsey and L. Kleinman, Phys. Rev. Lett. 39, 1297 (1977).
[41]The results in Ref. 29 are confirmed in G. V. Hansson and S. A. Flodström, Phys. Rev. B 18, 1562 (1978), and a surface resonance band is also reported for Al (111).
[42]See p. 35 of Ref. 25.